Beaching and Natural Removal Dynamics of Pelagic Sargassum in a Fringing-Reef Lagoon

Rutten, Jantien; Arriaga, Jaime; Montoya, Leonardo D.; Mariño-Tapia, Ismael J.; Escalante-Mancera, Edgar; Mendoza, E. Tonatiuh; van Tussenbroek, Brigitta I.; Appendini, Christian M.

DOI
10.1029/2021JC017636

Publication date
2021

Document Version
Final published version

Published in
Journal of Geophysical Research: Oceans

Citation (APA)
Rutten, J., Arriaga, J., Montoya, L. D., Mariño-Tapia, I. J., Escalante-Mancera, E., Mendoza, E. T., van Tussenbroek, B. I., & Appendini, C. M. (2021). Beaching and Natural Removal Dynamics of Pelagic Sargassum in a Fringing-Reef Lagoon. *Journal of Geophysical Research: Oceans*, *126*(11), Article e2021JC017636. https://doi.org/10.1029/2021JC017636

JGR Oceans

RESEARCH ARTICLE
10.1029/2021JC017636

Beaching and Natural Removal Dynamics of Pelagic Sargassum in a Fringing-Reef Lagoon

Jantien Rutten[1,2], Jaime Arriaga[1], Leonardo D. Montoya[1], Ismael J. Mariño-Tapia[3], Edgar Escalante-Mancera[4], E. Tonatiuh Mendoza[5], Brigitta I. van Tussenbroek[4], and Christian M. Appendini[1]

[1]Laboratorio de Ingeniería y Procesos Costeros, Instituto de Ingeniería, Universidad Nacional Autónoma de México, Sisal, México, [2]Now at Delft University of Technology, Faculty of Civil Engineering and Geosciences, Delft, The Netherlands, [3]Escuela Nacional de Estudios Superiores Unidad Mérida, Universidad Nacional Autónoma de México, Mérida, México, [4]Unidad Académica de Sistemas Arrecifales, Instituto de Ciencias del Mar y Limnología-UNAM, Puerto Morelos, México, [5]Normandie Univ, UNIROUEN, UNICAEN, CNRS, M2C, Rouen, France

Abstract Massive quantities of the pelagic brown macroalgae *Sargassum* spp. (sargassum) have been invading the Caribbean and West African shores since 2011, causing devastating effects on the coastal ecosystem and local economy. Little is known about sargassum beaching dynamics and the capacity of the coastal system to naturally remove beached sargassum. Here, we characterize the temporal variation in arriving and beached sargassum in a reef lagoon using a 5.2-year data set of hourly optical imagery, and identify the governing hydrometeorological conditions. Image classification reveals interannual variability in the start, duration, and intensity of the sargassum arrival season. Arrivals are associated with relatively low energy onshore directed winds and waves, and offshore abundance of sargassum. Furthermore, nearshore sargassum mat size is found to decrease with decreasing wave/wind energy. Once sargassum beaches, a berm of wrack is formed. Natural wrack removal was observed under elevated water levels and increased wave action. Three types of wrack removal were distinguished, depending on the water level η with respect to the berm crest height z_c and berm crest toe z_t: gradual berm destruction with gaps developing in the seaward berm edge that grow larger with time (Type I; $z_t < \eta < z_c$) and abrupt berm destruction with part of the wrack depositing on the upper beach (Type II; $\eta > z_c$) or in the dunes (Type III; $\eta \gg z_c$). Higher energy waves activate the reef circulation, which is suspected to flush part of the wrack out of the reef lagoon. We propose a conceptual model of nearshore sargassum dynamics in a reef lagoon system.

Plain Language Summary Unusually large masses of seaweed (*Sargassum* spp.) have been washing ashore along the Caribbean and West African coasts since 2011. The seaweed floods threaten coral reefs, seagrass beds, fish and turtles, and harm local economy as it discourages beach tourism. The seaweed, originating from the Atlantic Ocean, drifts in mats on the water surface with the ocean currents. It is unclear how seaweed arrives in nearshore waters and washes up the beach, and how long it resides once beached. We used hourly images of a reef lagoon (Puerto Morelos, Mexico) to study the beaching and natural removal of seaweed since 2015. The largest masses of seaweed beached in spring and summer of 2018 and 2019, whereas 2016 was hardly affected. Seaweed arrived under onshore directed weak winds and low waves, with the seaweed mat size increasing with weaker winds and lower waves. Higher waves and elevated water levels removed seaweed from the beach and brought it back in the water column. Seaweed was rapidly removed when the waves overtopped the seaweed deposit, and was removed gradually when waves reached only part of the deposit. Under high waves, the reef promotes currents that can flush seaweed out of the reef lagoon.

Key Points:

- Video monitoring allows the characterization of pelagic sargassum beaching and wrack dynamics
- Sargassum deposits are removed from the beach and resuspended under elevated water levels and increased wave action
- Nearshore sargassum mat size decreases with increasing wave and wind energy

Correspondence to:
J. Rutten and C. M. Appendini,
j.rutten@tudelft.nl;
cappendini@iingen.unam.mx

Citation:
Rutten, J., Arriaga, J., Montoya, L. D., Mariño-Tapia, I. J., Escalante-Mancera, E., Mendoza, E. T., et al. (2021). Beaching and natural removal dynamics of pelagic sargassum in a Fringing-reef lagoon. *Journal of Geophysical Research: Oceans*, *126*, e2021JC017636. https://doi.org/10.1029/2021JC017636

Received 3 JUN 2021
Accepted 18 OCT 2021

Author Contributions:

Conceptualization: Jantien Rutten, Jaime Arriaga, Ismael J. Mariño-Tapia, Christian M. Appendini
Data curation: Jaime Arriaga, Edgar Escalante-Mancera, E. Tonatiuh Mendoza
Formal analysis: Jantien Rutten, Leonardo D. Montoya
Funding acquisition: Jaime Arriaga, Christian M. Appendini
Investigation: Jantien Rutten, Leonardo D. Montoya
Methodology: Jantien Rutten, Jaime Arriaga, Leonardo D. Montoya, Christian M. Appendini
Project Administration: Christian M. Appendini

1. Introduction

Extraordinarily large quantities of the pelagic brown macroalgae *Sargassum* spp., consisting of species *S. fluitans* and *S. natans* and hereafter referred to as sargassum, invaded the shores of the Caribbean and tropical West Africa in 2011 (Franks et al., 2012; Gower et al., 2013) and have been reoccurring since then (Johns et al., 2020; Wang et al., 2019). Drifting on the ocean surface, sargassum provides shelter and habitat for marine species (e.g., fish, shrimp, crab, and turtles). Once arriving in nearshore waters and washing ashore,

Resources: Edgar Escalante-Mancera, Christian M. Appendini
Software: Jantien Rutten, Jaime Arriaga, Leonardo D. Montoya
Supervision: Jaime Arriaga, Christian M. Appendini
Validation: Jantien Rutten, Jaime Arriaga, Leonardo D. Montoya, Christian M. Appendini
Visualization: Jantien Rutten, Leonardo D. Montoya
Writing – original draft: Jantien Rutten
Writing – review & editing: Jantien Rutten, Jaime Arriaga, Leonardo D. Montoya, Ismael J. Mariño-Tapia, Edgar Escalante-Mancera, E. Tonatiuh Mendoza, Brigitta I. Tussenbroek, Christian M. Appendini

the massive quantities are highly problematic, affecting negatively the coastal ecosystem, local economy, and human health. For instance, seagrass and coral mortality has been observed to increase due to decreasing light, PH, and oxygen levels in nearshore waters, associated with the decaying sargassum masses on the beach (Van Tussenbroek et al., 2017). Also, fish and crustacean mortality have been related to increased ammonium and hydrogen sulfide concentrations and hypoxia in reef lagoons (Rodríguez-Martínez et al., 2019), and nesting of turtles has been hindered due to the sargassum masses on the beach and in shallow water (Maurer et al., 2015, 2019). Besides, local economies suffered with a reduced income as a result of a lower number of beach visitors during the sargassum season and costs associated with artificial sargassum removal (Chávez et al., 2020). These examples illustrate the urgent need to better understand and, consequently, manage the recent massive sargassum beachings.

In the last decade, considerable insights have been gained on the massive sargassum influx from an oceanographic perspective. The recent massive beachings in the Caribbean and West Africa were found to relate to a sargassum population north of the equator in the tropical Atlantic (Franks et al., 2012, 2016; García-Sánchez et al., 2020; Gower et al., 2013; Johnson et al., 2013), which established in 2010/2011 due to anomalous winds in the northeast Atlantic related to the North Atlantic Oscillation (Johns et al., 2020) alongside of the known sargassum populations in the Sargasso Sea and the Gulf of Mexico (Gower & King, 2011). Particle backtracking revealed oceanographic pathways of sargassum from the Tropical Atlantic into the Caribbean Sea, following oceanographic currents and winds (Franks et al., 2016; Johns et al., 2020; Johnson et al., 2013; Putman et al., 2018; Wang et al., 2019). Satellite imagery showed that the distribution of sargassum in the Tropical Atlantic and Caribbean Sea varied seasonally and interannually (Johns et al., 2020; Wang & Hu, 2016; Wang et al., 2019). The temporal variability has been suggested to relate to variability in currents, winds, sea surface temperatures, nutrients, and the sargassum lifecycle (Johns et al., 2020; Wang et al., 2019). Presumably, the ocean dynamics of sargassum are reflected in beaching events.

So far, few studies have investigated sargassum beaching. García-Sánchez et al. (2020) carried out an in situ monitoring campaign, sampling the fresh sargassum wrack at the beach of the Puerto Morelos reef lagoon (Mexico) on weekly to biweekly basis over a 3.8-year period. The authors found a seasonal and interannual variability in beached biomass, which they related to variability in abundance of sargassum in the nearby ocean current and local wind climate. Also, Putman et al. (2020) suggested that, besides surface currents, winds play an important role in sargassum transport from the open ocean to the nearshore, and thus in the location of beaching. So far, little is known about the dynamics and fate of sargassum wrack. Despite the recognition of the problematic ecosystem effects of massive quantities of sargassum wrack, residence times of the wrack are hardly known. Furthermore, the capacity of a coastal system to remove massive quantities of wrack, through decomposition or removal by wind, waves or currents, has not been thoroughly investigated.

To quantify wrack dynamics and relate events of wrack deposition and removal to hydrometeorologic conditions, long-term high-resolution data sets are required. In situ monitoring of sargassum wrack provides accurate data but is time consuming, which often leads to compromised sampling resolutions and monitoring periods. Furthermore, satellites have been shown helpful to study ocean dynamics of sargassum, serving as addition and/or alternative to labor-intensive in situ campaigns. However, resolutions of satellite imagery are too coarse to investigate sargassum dynamics in the nearshore, where scales of variability are smaller and near-continuous monitoring is required. Here, land-based video stations can be used as they efficiently provide hourly information of the beach and nearshore with a pixel footprint of $O(1)$ m, allowing long-term monitoring (Holman & Stanley, 2007). Sargassum pixels can be identified with machine learning techniques, as explored by Berriel-Bueno (2018), Arellano-Verdejo et al. (2019), Valentini and Balouin (2020), and Arellano-Verdejo and Lazcano-Hernández (2021). Here, we present a 5.2-year data set of hourly images, collected from the Puerto Morelos reef lagoon (Mexico) that has been affected by massive sargassum beaching since late 2014 (Figures 1a and 1b). In this study, we characterize the temporal variability in sargassum wrack dynamics, and identify the hydrometeorological conditions that govern these dynamics. Section 2 describes the study site, data sets and classification methods. Section 3 presents our results on sargassum arrivals, wrack removal and wrack coverage. Section 4 discusses sargassum arrival and wrack dynamics, and proposes a conceptual model. Section 5 presents the main conclusions.

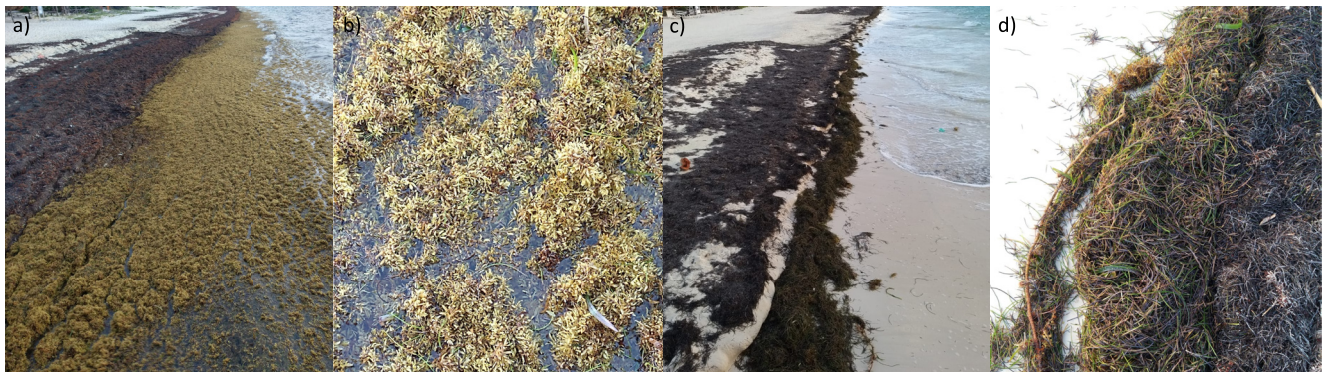

Figure 1. Beached (a, b) sargassum on May 2021 and (c, d) seagrass on January 29, 2021 near the video monitoring station in Puerto Morelos. Photos were taken by Amador Hernández Gómez.

2. Methodology

2.1. Field Site

The study was performed at the beach of Puerto Morelos (20.8662°N, 86.8686°W), located 20 km south of the tropical beach resorts of Cancun, Mexico (Figure 2). The beach is NE-SW oriented (20°), composed of carbonate sand of biogenic origin with a mean grain size of 300 μm (Ruiz de Alegria-Arzaburu et al., 2013), and is located in a reef lagoon. The reef is part of the Mesoamerican Barrier Reef System (MBRS), which extends along the Caribbean coast of Mexico, Belize, Guatemala, and Honduras. The MBRS is discontinuous with open exposed beaches in between beaches sheltered by a reef. The reef system at the study site consists of a shallow back-reef lagoon (on average 3.5 m deep) of 550–1,500 m wide, a reef with variable crest depth (Torres-Freyermuth et al., 2012), and a gently sloping forereef that ends in a sandy platform at 20–25 m depth. The shelf edge is located at 40–60 m depth. The reef is dissected by two inlets of 6 m deep (north), and an 8 m deep dredged, navigational channel (south; Figure 2). The sandy bottom of the reef lagoon is colonized by seagrass (*Halodule wrightii*, *Thalassia testudinum*, and *Syringodium filiforme*) and rooted macroalgae (Van Tussenbroek, 2011).

The study site is exposed to a trade wind regime with NE-SE winds of 6–9 m/s, tropical storms and hurricanes (June–November) and 2–5 days events from the north that are related to anticyclonic cold fronts (October-April, Appendini et al., 2018). The wave climate is characterized by low-energetic E-SE waves with a peak period T_p of 5–9 s and a significant wave height H_s of 0.5–1.5 m. Wave energy increases during cold fronts (H_s = 2–3 m, T_p = 6–11 s) and tropical storms and hurricanes ($H_s > 2.5$ m, $T_p > 8$ s). Tides are semidiurnal with a mean tidal range of 0.17 m and a neap and spring tidal range of 0.07 and 0.32 m, respectively (Coronado et al., 2007). The Yucatan Current, with its core located 12 km offshore from the study site, flows to the northeast with a speed that varies between 2 m/s in summer (April–November) and 0.9 m/s in winter (December–March). Coronado et al. (2007) suggested that coastal water levels fluctuate at subinertial frequencies with the intensity of the Yucatan Current, lowering under an enhanced current through geostrophic coupling. They observed that circulation in the reef lagoon system is predominantly wave-driven. Wave breaking on the forereef induces a water level setup on the reef, creating a pressure gradient that drives a shoreward flow across the shallow back-reef lagoon and a return flow through the inlets. At the study site, the net alongshore current is to the north-northeast. Measurements show that the tide modulates the flow field inside the lagoon, enhancing the current toward the NNE during ebbing and weakening the current during flooding.

2.2. Image and Field Data

A 5.2-year data set (September 2015–November 2020) of hourly images has been collected during daylight by a land-based video station. The station was mounted atop a 15 m high building, and consisted of two cameras looking southward along the beach. Oblique images (1,280 × 960 pixels) were converted into plan-view images, allowing quantitative analysis of fresh sargassum arrivals and wrack. This is done by relating

Figure 2. Location of the study site.

the pixel positions of discernible features to surveyed Ground Control Points in UTM coordinates (Simarro et al., 2017). Afterward, images were projected (rotation and translation) on a local Cartesian coordinate system with the x axis directed offshore, the y axis directed southwesterly along the beach, and z constant at 0 m. During 7% of the study period no images were collected due to technical issues, with the longest data gap from October 19 to 27, 2015. The arrival of sargassum mats in the nearshore (<200 m from the shoreline) were analyzed from snapshot images that covered 250 by 250 m in the cross-shore and alongshore direction with a grid size of 0.2 m. Beached sargassum, referred to as wrack, was quantified from time-averaged images, created from 10 min recordings sampled at 2 Hz. These images allowed quantification of wrack coverage without dependencies on the beach width as the swash-induced motion of the waterline was averaged out. Images covered 60 by 100 m in the cross-shore and alongshore direction and had a grid size of 0.1 m.

Hourly estimates of offshore significant wave height H_s, peak period T_p, and mean wave direction θ were obtained from the nearest node (21.0°N, 86.5°W) of the ERA5 hindcast (generated by Copernicus Climate Change Service; https://cds.climate.copernicus.eu/). Onsite measured wind speed u_{wind} and wind direction θ_{wind} data with hourly resolution were obtained from SAMMO (https://sammo.icmyl.unam.mx/). Water levels η, measured every minute, were obtained from Servicio Mareográfico (http://www.mareografico.unam.mx/portal/). Preprocessing of the water level data included removal of outliers, linear interpolation when data gaps were small (<180 min), smoothing with a 1 h Gaussian-shaped window, and hourly extraction of

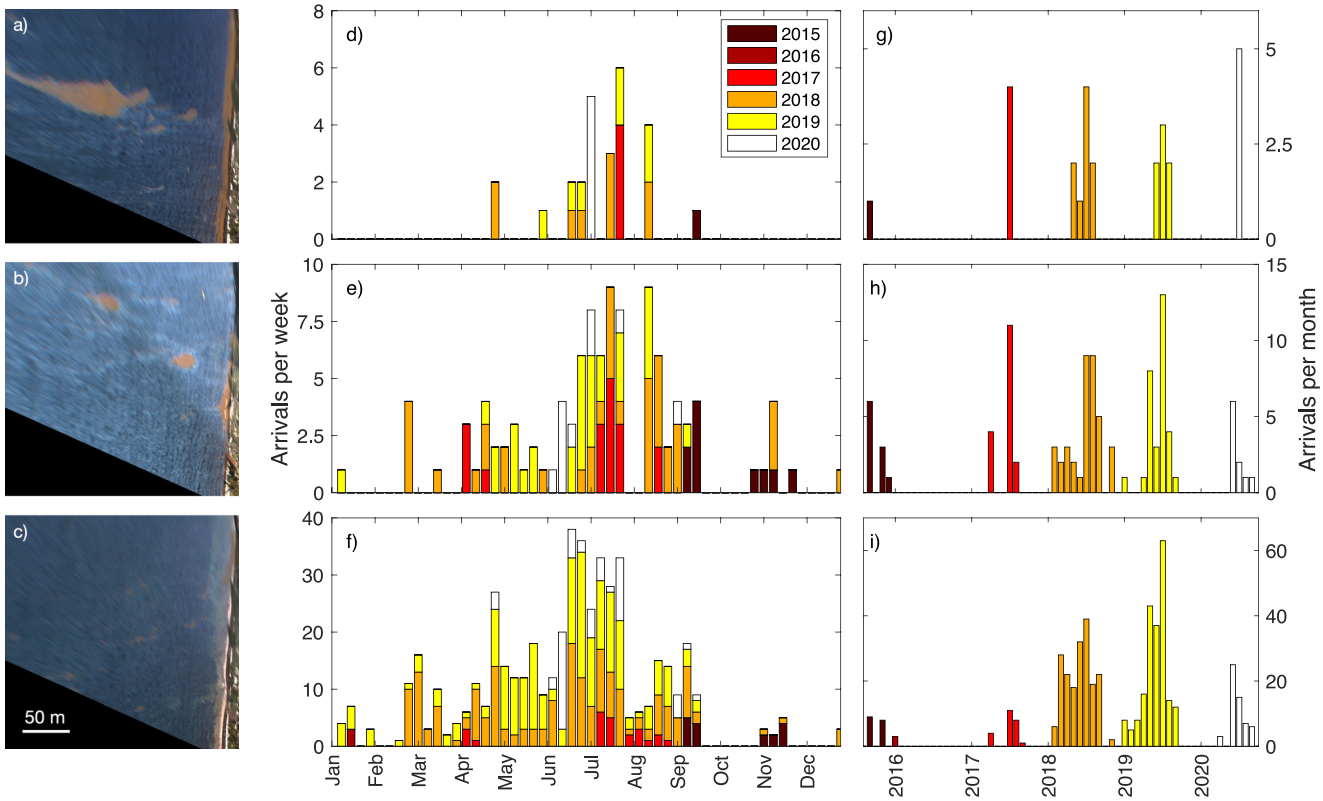

Figure 3. Example snapshot images that show a typical (a) large, (b) medium, and (c) small arrival, and variability in number of (d, g) large, (e, h) medium, and (f, j) small arrivals on (d–f) annual and (g–i) interannual timescales.

data points. Wind and water level data were not available 11% and 4% of the time, respectively. The offshore wave energy imposed on the reef lagoon system was characterized by the wave power P, computed as

$$P = \frac{\rho g^2}{32\pi} H_{rms}^2 T_p, \tag{1}$$

with sea water density ρ of 1,025 kg/m^3, gravitational acceleration g of 9.81 m/s^2, and root-mean-square wave height H_{rms}.

2.3. Arrival and Wrack Classification

Arrivals were characterized by selecting images with sargassum mats on the water surface and dividing them in three classes. Images with large, medium and small arrivals were distinguished (Figures 3a–3c), based on visual estimation of the size and number of the mats in every image. Images with 1–3 mats with a large diameter (>35 m) or several mats with a medium diameter (10–20 m), reaching a total surface area of more than 1,500 m^2, were classified as large arrivals. Images with several mats with a medium diameter and a total surface area of more than 200 m^2 were classified as medium arrivals. Images with a single mat with a medium diameter or tens of small, near-circular mats with a diameter of 2–6 m and a total surface area below 200 m^2 were classified as small arrivals. Images with mats smaller than 2 by 2 m were not included in the image selection because they could be easily missed under poor imaging conditions or rough seas. An attempt to automatically detect arrivals was unsuccessful due to large differences in the color of the mats, color of the water and sea state in the images. Sargassum mats that arrived overnight were missed, along with those arriving in between sample moments or during poor image conditions (e.g., sun glare, rough seas). Therefore, the classification serves only as rough indicator of sargassum arrivals.

Temporal variability in wrack coverage was analyzed from a timestack of a single image transect for the 5.2-year study period with pixels of 0.1 by 0.1 m. Wrack pixels were detected with a Support Vector Machine (SVM) classifier, which relies on the estimation of a hyperplane that separates two classes in multi-dimensional feature space. Similar techniques have been applied to classify pixels in oblique images of the coastal zone (Hoonhout et al., 2015; Valentini & Balouin, 2020). Here, the SVM classifier separated wrack pixels from other pixels using redness, greenness, blueness, and cross-shore position of the pixels. First, the SVM classifier was trained with 158 wrack pixels and 116 pixels of the beach, water and foam that were manually picked (Jantien Rutten). Second, pixels in the timestack were classified using the trained SVM classifier. Vegetation pixels were masked to prevent false classification of vegetation as wrack. Wrack coverage followed from the number of wrack pixels multiplied by the pixel size. Third, the SVM performance was evaluated with a confusion matrix, commonly used to assess how classifications compare with ground truth. Hereto, 300 pixels were picked randomly from the timestack image. Pixels were only picked near the shoreline (strip of 12.5 m) to obtain a sufficiently large group of wrack pixels, resulting in 70 wrack pixels and 230 nonwrack pixels. Subsequently, ground truth pixel labels were assigned (Jantien Rutten). Then, 300 ground truth and predicted labels were compared, providing true positives (TP), true negatives (TN), false positives (FP), and false negatives (FN). These results were summarized by computing the precision $P = TP/(TP + FP)$, sensitivity $S = TP/(TP + FN)$, and F score $F1 = 2PS/(P + S)$.

3. Results

3.1. Arrival and Beaching

Sargassum mats detected in nearshore waters varied in shape, size, number, and color. Mats were often oval-shaped with a tail, but also elongated, circular and irregular-shaped mats were observed (Figures 3a–3c). Mats measured from 2 by 2 m, up to 30 by 60 m. The number of mats varied from one to tens (for image of 250 × 250 m). Possibly, the mat color gives an indication of the mat density or thickness, as bright brown colors may be caused by accumulations of sargassum and paler colors to sargassum interspersed with water. In addition, the freshness of sargassum, presence of other vegetation or debris and image light conditions can play a role in mat color. Commonly, golden is used to describe the color of fresh sargassum. Five-year arrival identification and classification yielded 625 arrivals out of 25,298 images, revealing that a season of arrival can be distinguished from March to the beginning of September with a peak in July when several large events occur per week (Figures 3d–3f). Small and medium arrivals preceded and followed up large arrivals. Nearly no sargassum arrived between October and mid-February. Furthermore, interannual variability in arrivals can be distinguished, with peak years in 2018 and 2019 and an extremely mild year in 2016 (Figures 3g–3i). In 2017 and 2020, arrivals were roughly concentrated between June and August. In 2018 and 2019, the duration of the arrival season was similar (7 months; March–September), but a higher number of large and medium events were found in 2018 in comparison to 2019, with 9 versus 7 and 37 versus 31 events, respectively.

Wave and wind conditions related to the arrivals (preceding 6 h to arrival observation; Figures 4c–4e and 4h–4j) are on average less energetic than the average conditions found throughout the arrival season (March-August; Figures 4b and 4g). More particularly, the range and average of H_s are smaller (0.4–1.6 and 0.9 m versus 0.4–2.2 and 1.1 m). Besides, average H_s is smaller for large arrivals (0.7 m) than medium (0.9 m) and small arrivals (1.0 m). In contrast, T_p is similar for arrivals and for the arrival season (7 s; not shown). Also θ is largely similar, with averages of 103 and 105° and with 99% and 97% of the conditions being within the range of 30–130° (Figures 4k and 4l). However, the peak wave direction of 110° is clearly more predominant (58% versus 44%). In line with trends in H_s, u_{wind} has a narrower range and lower average for individual arrivals than for the entire arrival season (1–9 m/s versus 1–11 m/s; 5.1 m/s versus 5.7 m/s) and decreases with increasing arrival size (Figures 4h–4j). The range of θ_{wind} is not substantially different, but the average θ_{wind} is more shore-normal (107 versus 125°; Figures 4m and 4n).

If mats drifted in shoreward direction, sargassum accumulated in coastal waters and washed ashore, hereafter referred to as beaching. Figure 5 shows an example time-averaged image with beaching sargassum. The dark brown strip along the beach is a wrack berm of a previous beaching event. The vague light brown band is related to large quantities of slowly moving, floating sargassum, that is the sargassum color smoothed out over the pixels where sargassum passed during the 10 min recording of the time-average image. An example

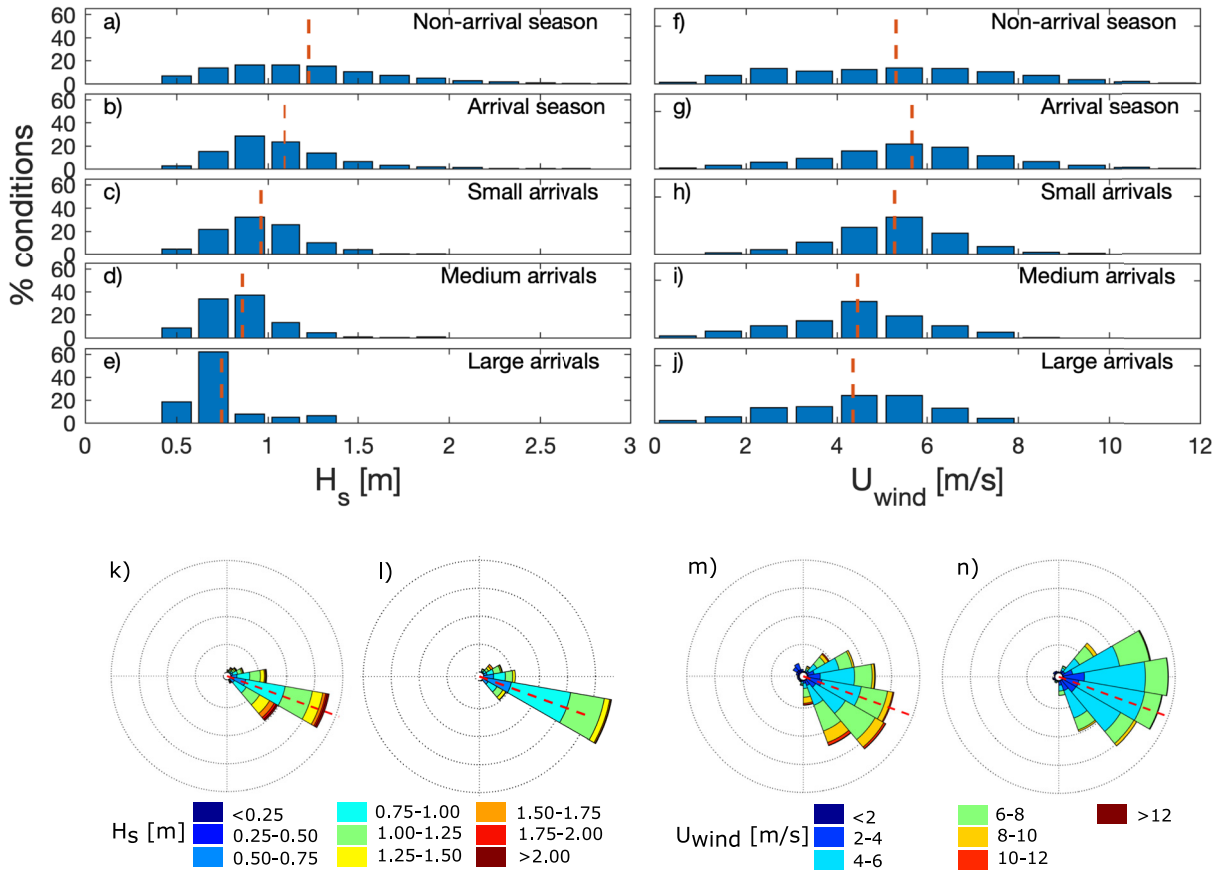

Figure 4. Occurrence of (left) wave height H_s and (right) wind speed U_{wind} conditions for the (a, f) study period, (b, g) arrival seasons, (c, h) small arrivals, (d, i) medium arrivals, and (e, j) large arrivals. The vertical dashed lines indicate the average condition. Wave and wind roses of the (k, m) arrival season and (l, n) all arrivals are shown, with the red dashed line indicating the shore-normal direction at the study site.

of a beaching event is illustrated in Figure 6 with a series of hourly images. Initially, the band of floating sargassum grew seawards with the incoming arrivals (12:00–16:00), reaching a maximum cross-shore extension of 12 m at 17:00. Then, floating sargassum started beaching (from 18:00 onwards) and the band of floating sargassum slowly disappeared. The freshly beached sargassum can be observed in Figure 6 as a red brown strip along the old wrack berm. Observations show that beaching events of similar size happened several times within the study period (2018: 10 events; 2019: 6 events) and typically lasted a few hours. Particularly large quantities beached when 2–3 events followed up each other within a few days, resulting in wide wrack berms. Smaller beaching events, often without the presence of light brown-colored water caused by slowly moving sargassum, were observed more frequently throughout the study period.

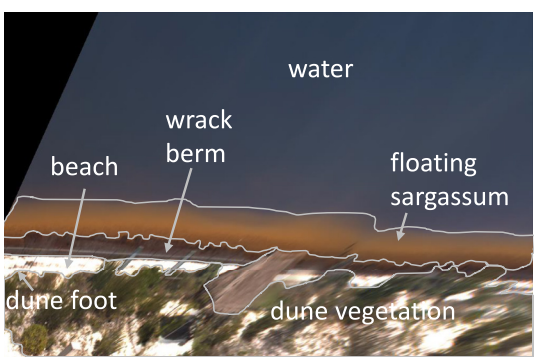

Figure 5. Example time-averaged image on June 5, 2019 18:00 with floating sargassum, wrack berm, beach, water, and vegetation indicated by arrows.

3.2. Wrack Removal

Images show that wrack was artificially and naturally removed from the beach. Images were visually inspected to detect artificial clean-up campaigns (oblique snap shots) and natural wrack removal (planview time exposures). During the study period 18 artificial clean-up campaigns were observed, including 14 campaigns in 2018 (July–December) 3 in 2019 (January, August) and 1 in 2020 (September). Different natural removal mechanisms were distinguished: gradual berm destruction with gaps developing in the seaward berm edge that grow larger with time

Figure 6. Time-averaged images on June 5, 2019 showing beaching of sargassum.

(Type I) and abrupt berm destruction with part of the wrack depositing on the upper beach (Type II) or in the dunes (Type III). Here, the dunes were defined from the vegetation line inland, used to distinguish Type II from Type III events.

The Type I removal mechanism was only observed in the arrival season, when large wrack berms were located at the lower beach and water levels were relatively low. Figure 7 shows an example of Type I removal. Small gaps appeared along the seaward edge of the berm with rising tide and increasing wave action, as pieces of wrack were brought back in the water column (i.e., resuspension). Subsequently, gaps grew larger during consecutive rising tides, until a beaching event filled up the gaps (Figure 7a: June 8, 2019 11:00) or until the entire wrack berm was removed (Figure 7a: June 10, 2019). In 2019, 21 of these events were observed, all during moderate energy conditions ($P < 11.8$ kW/m, $U_{wind} < 10.4$ m/s) and water levels $1.17 < \eta < 1.32$ m.

Type II removals were observed 16 times throughout the study period, all during elevated water levels (>80th percentile; $1.31 < \eta < 1.55$ m) and higher energy conditions ($5.0 < P < 37.2$ kW/m; $7.7 < U_{wind} < 14.6$ m/s; Figure 8). As a result, the swash zone moved inland (Figure 8a: February 6, 2020 12:00), allowing resuspension of the wrack berm and deposition of part of the wrack higher on the beach along the vegetation line 0.5–3 days later. Most events occurred in October-November (38% of the events), when the water level was high because of geostrophic coupling. Generally, thin wrack lines appeared on the lower beach several days after wrack deposition on the upper beach, when the water level decreased (Figure 8a).

Type III removal is similar to Type II but with wrack deposition further inland, into the dunes. Ten Type III removals were observed, all during high energy wave conditions ($P > 39.7$ kW/m) and extreme water levels ($\eta > 1.42$ m; 97th percentile), provoking the further inland deposition of wrack. Part of the dune vegetation was removed or buried with sand during the more energetic events (Figure 8b: October 20 12:00). The extremely energetic event in October 2020, an anomaly in the 5.2-year study period caused by the landfall of a hurricane, removed wrack from the beach and largely destroyed the dune vegetation (Figure 8c: October 28 20:00). Wrack deposits (Type II and III) can have a positive effect on dune vegetation (Del Vecchio et al., 2017). Further study on the impact of increased wrack deposition on dune vegetation is suggested.

3.3. Wrack Coverage and Residence Time

Although sargassum beached mainly between March and September, wrack was present for nearly the entire study period. Figure 9a reveals the temporal variability in the quantity and cross-shore position of wrack. Wrack can be distinguished as dark brown pixels located landward from the white band caused by

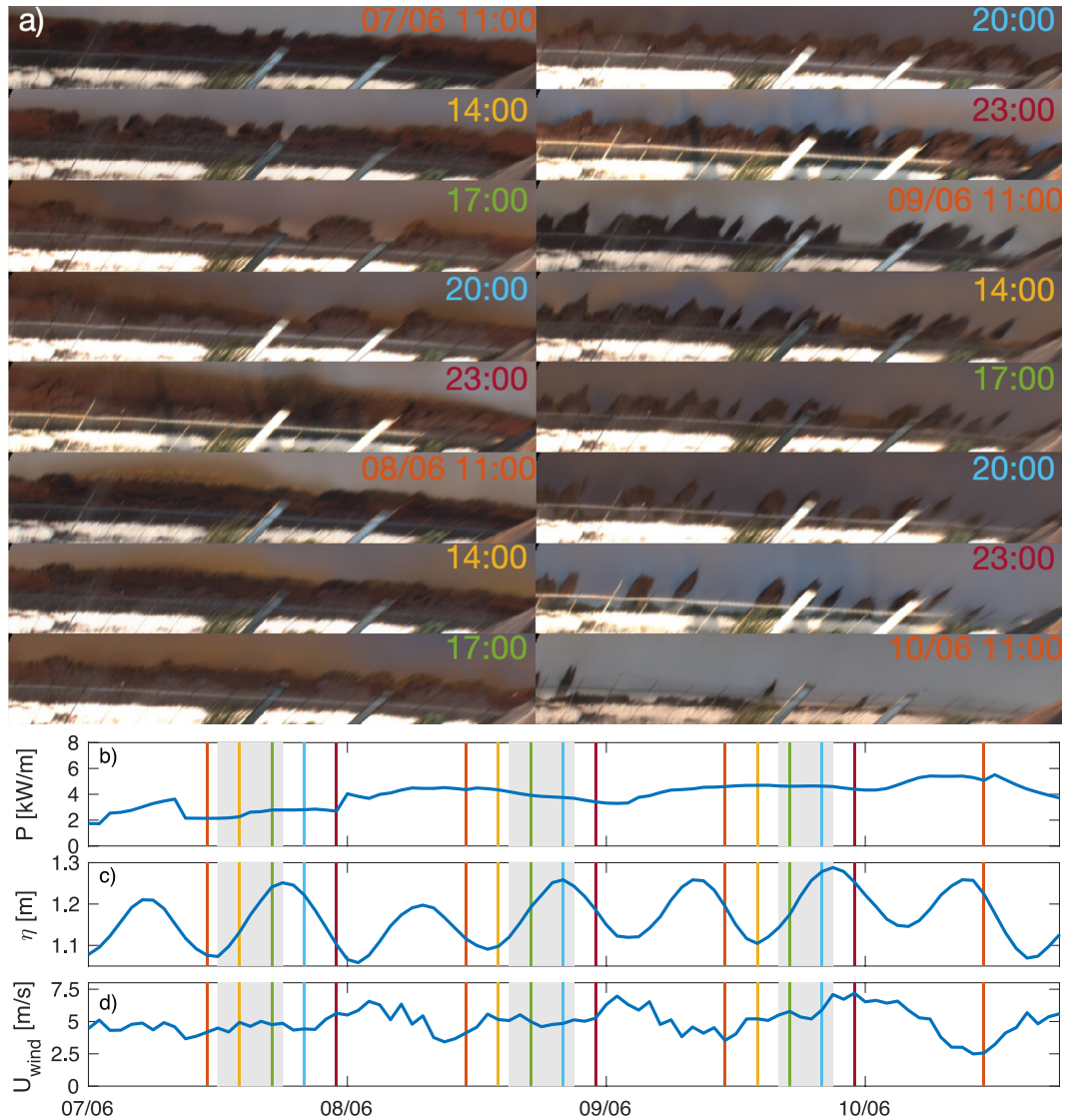

Figure 7. (a) Time-averaged images from June 7 to 10, 2019 showing destruction of wrack berm with corresponding, (b) wave power P, (c) water level η, and (d) wind speed U_{wind}. Colored vertical lines in (b–d) correspond to the images, whereas gray shadings indicate periods of wrack berm destruction.

white foam in the swash zone. Wrack pixels were detected with the SVM classifier with reasonable accuracy, illustrated by the red contour (Figure 9a) and the confusion matrix metrics ($TP = 55$ and $TN = 230$, $FN = 15$, $FP = 0$, $P = 1$, $S = 0.79$, and $F1 = 0.88$). The nonnegative FN indicates that not all wrack pixels were recognized by the SVM classifier, whereas zero FP demonstrates that no pixels in the 300-pixel sample were wrongly classified as wrack. Thus, these metrics provide indications that wrack coverage is rather under-than overpredicted.

Wrack coverage is typically larger in the arrival season than in the rest of the year (Figure 9b), which can be explained by the respective variability in wrack arrival and removal. After the first big beaching of the year, the landward limit of wrack is typically stable for several months (e.g., May-August 2019) and the upper beach remains wrack-free. This suggests that coverage variability in the arrival season is predominantly caused by wrack dynamics along the waterline, including beaching and berm destruction (Type I). Higher on the beach, wrack resides for months. Only 5 times a reset of the landward limit is observed in the arrival seasons, which were caused by artificial removal of wrack (blue lines; July 2018, August 2019) or by deposition of wrack in the dunes during Type III events (red lines; June 2017, August 2017, June 2020) or at the

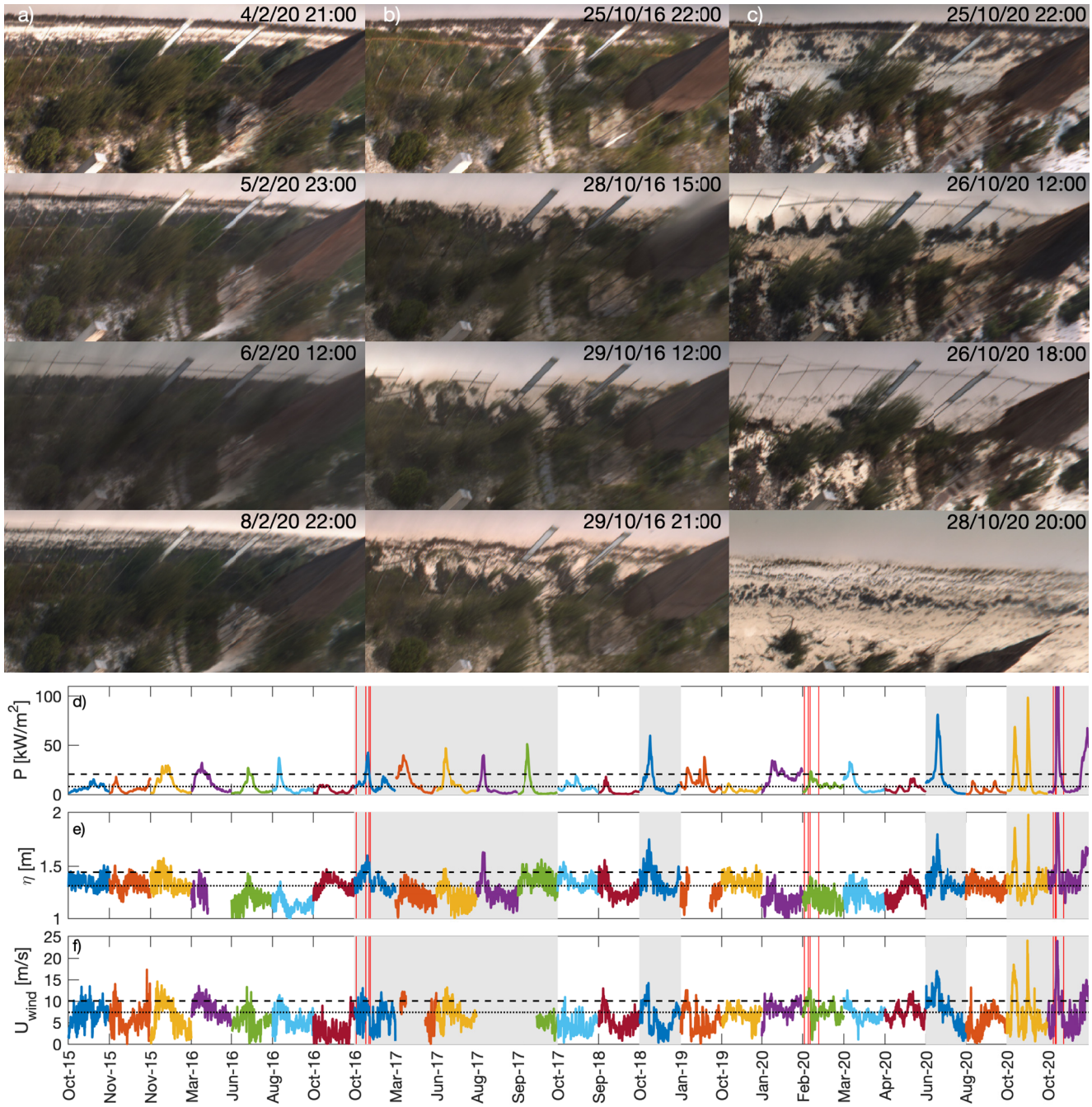

Figure 8. Time-averaged images showing examples of (a) Type II removal with deposition of wrack at the dune foot, (b) Type III removal with deposition of wrack into the dunes, and (c) extreme event with vegetation destruction, and conditions during all Type II (white shading) and Type III (gray shading) events with (d) wave power P, (e) water level η, and (f) wind speed U_{wind}. Colors and $x-$ axis labels in (d–f) correspond to the individual events, red vertical lines correspond to the date of the images, and horizontal dotted and dashed lines indicate the 80th and 97th percentiles.

dune foot during Type II events (yellow lines; April 2020). Typically, wrack is observed again within a few days. Outside the arrival season, wrack dynamics are different. Coverage changes due to wrack variability along the waterline, but more importantly due to Types II and III removal. Wrack remains at the dune foot until it is displaced further into the dunes (e.g., October 2016) or overgrown by vegetation (e.g., June 2017, January 2018), leading to residence times of up to 100 days (March-June 2017).

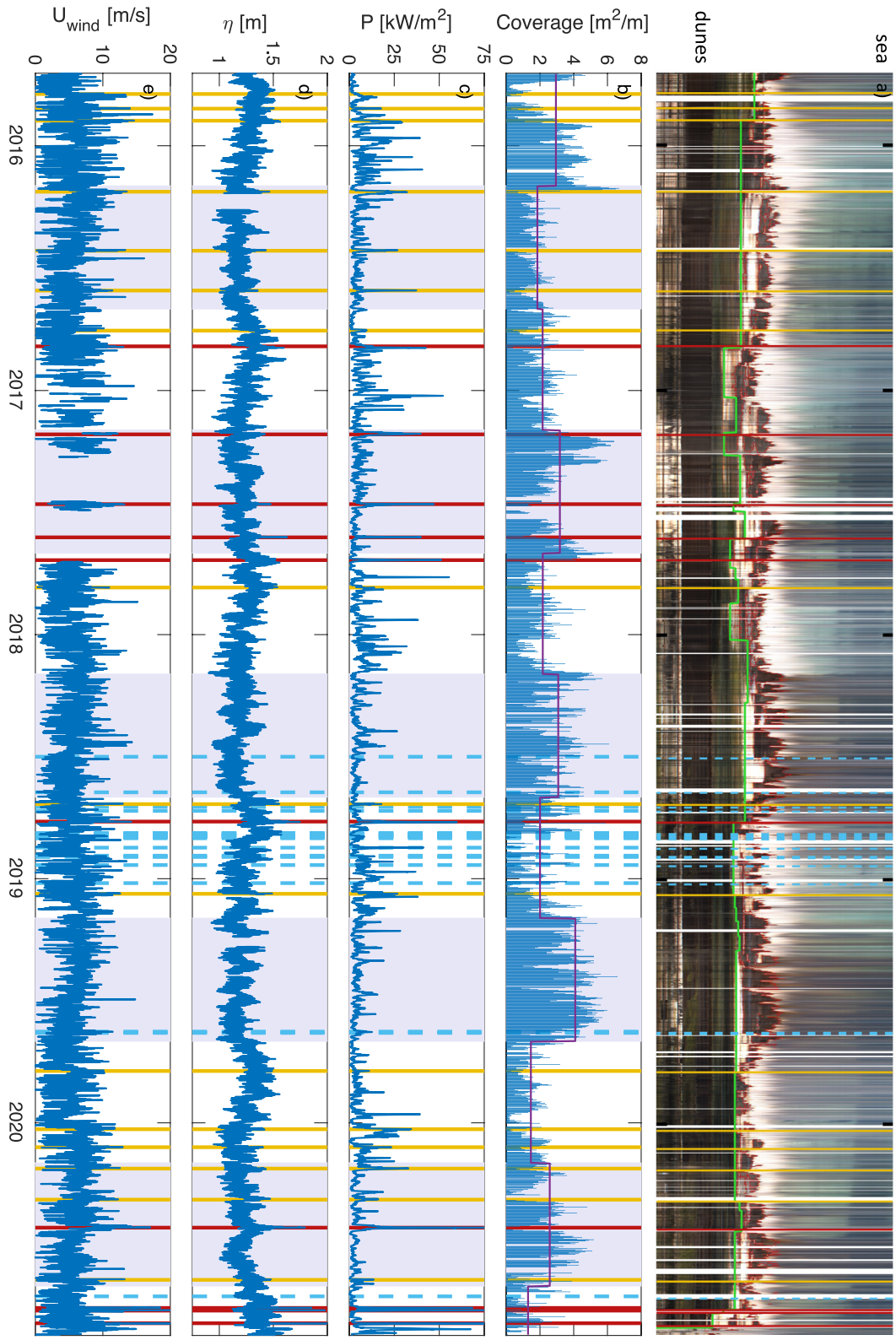

Figure 9. (a) Timestack of daily pixel transects of time-averaged images, (b) wrack coverage computed from detected wrack pixels in (a; red contour), (c) wave power P, (d) water level η, and (e) wind speed U_{wind}. Vertical lines indicate Type II removal (yellow), Type III removal (red), and artificial removal (dashed blue). Gray shadings in panels (b–e) indicate the arrival season from March to September. The green line in panel (a) indicates the vegetation line, whereas the purple line in panel (b) indicates the average coverage in the arrival and nonarrival seasons.

Wrack coverage also varies at interannual timescales, with large values in the arrival season of 2019, moderate in the arrival season of 2017, 2018, and 2020 and small values in 2016 (purple line in Figure 9b). In 2018, several clean-up campaigns and a relatively seaward located berm resulted in only moderate wrack coverage, despite the many beaching events (Section 3.1). In 2017, old wrack from the preceding winter was still located on the upper beach when large quantities started beaching (Figure 9a), resulting in large coverage values in March. Furthermore, coverage was large in the winter of 2015 compared to the other winters. In September 2015, large values are related solely to large beaching events (Figure 9a). Later in winter, arrivals but also wrack that deposited on the upper beach during the Type II event in November (yellow line) caused high coverage.

4. Discussion

4.1. Arrival Dynamics

Imagery reveals that most sargassum arrives and beaches at Puerto Morelos between March and September, with peak quantities in July. Earlier, García-Sánchez et al. (2020) found at the same beach a similar seasonality from biomass measurements of freshly beached sargassum. The overlapping monitoring period of the biomass measurements with our image data set from September 2016 to May 2020 allows to compare interannual variabilities. Both data sets indicate 2018 and 2019 as peak years, but only the image data set suggests that 2017 was a moderate year with several arrivals per week in July and August. An interruption of biomass monitoring (June-August 2017) during the arrival season explains why 2017 was considered a mild year in García-Sánchez et al. (2020).

García-Sánchez et al. (2020) suggested that the seasonal signal in beaching can be explained by variability in the abundance of sargassum in the Yucatan Current and the wind climate. The authors showed that sargassum observed in the Yucatan Current did not beach in Puerto Morelos if $180 < \theta_{wind} < 60°$ prevailed the day before wrack collection, and suggested that the northerly winds in autumn and winter prevented shoreward drift of sargassum in that season. Also Putman et al. (2020) suggested that winds can play an important role in beaching, based on a tracking experiment near the Dominican Republic (North Caribbean). They showed that the path of GPS-tracked sargassum mats was followed more accurately by synthetic particles released from the same offshore location at the open ocean, when including wind in model predictions. Consequently, beaching locations were predicted more accurately. The importance of the local wind climate on the seasonal variability in beaching at Puerto Morelos can be further explored with our data set, which is unique in its temporal resolution (hourly daylight observations) and extension (five arrival and five nonarrival seasons).

During the study period, 625 sargassum arrivals were observed in the nearshore, and, in line with García-Sánchez et al. (2020), were associated with winds ranging from the north-northeast to south. Presumably, northwestern winds drive sargassum away from the NNE-SSW oriented beach, explaining why no arrival and beaching was observed under such wind directions. However, the few arrival observations from September to March cannot solely be explained by the wind direction, as analysis of 5.2-year wind data with hourly resolution indicates that northwestern winds are more common in these months than in the arrival season (38% versus 16% occurrence) but that eastern winds still dominate (62%). Besides eastern winds, arrivals were associated with relatively low-energetic wave and wind conditions, and E-SE waves (Figure 4). Possibly, the shore-normal (E-SE) waves stimulate shoreward drift, whereas low-energetic conditions may help to preserve the cohesion of sargassum mats. To the contrary, higher waves and stronger wind may break mats in smaller chunks, which could explain the observed higher energetic conditions for smaller arrivals (Figure 4). Considering the ranges of H_s, u_{wind}, θ, and θ_{wind}, prevalent arrival conditions were less frequent in autumn and winter than in the arrival season but not uncommon (48% versus 63% occurrence). Therefore, we suggest that the lack of arrival observations in autumn and winter relates largely to seasonal differences in offshore sargassum abundance. Satellite data demonstrated seasonal variability in sargassum abundance in the western Caribbean Sea, in general with low quantities in January and peak quantities in July (Chávez et al., 2020; Johns et al., 2020; Trinanes et al., 2021; Wang et al., 2019). Data with high temporal resolution (minutes) and large footprint (km^2), providing drift direction and velocities of sargassum under a large range of hydrodynamic conditions, can give further insight in the conditions that govern sargassum drift from the ocean to the beach. Such insight is also essential for the improvement of sargassum early warning

systems (Hu et al., 2016; Maréchal et al., 2017; Trinanes et al., 2021; Webster & Linton, 2013), which provide information that can help coastal communities to better manage massive sargassum beachings.

4.2. Year-Round Wrack Coverage

Wrack covered the beach nearly permanently (Figure 9), despite seasonality in sargassum influx (arrivals from March to September) and year-round wrack removal (Types I–III). We raise two hypotheses that together can explain the near-permanent wrack presence.

First, wrack of different species deposits outside the sargassum arrival season. Field observations indicate that winter wrack consists predominantly of seagrass (Figures 1c and 1d) and hardly of pelagic *Sargassum* Spp. (García-Sánchez et al., 2020). Increased wave action, occurring more frequently in winter at our site (Figure 9c), stimulates breakage of seagrass leaves. The response of seagrasses is species specific. Fourqurean and Rutten (2004) found that a hurricane of moderate strength in the Florida Keys caused larger losses in density of *S. filiforme* and calcaerous green algae than of *T. testudinum*. They suggested that early successional species (e.g., *S. filiforme*) are more vulnerable for leaf breakage than late-successional species (e.g., *T. testudinum*). Furthermore, Williams (1987) showed that the leaves of *S. filiforme* can be protected from breakage by the canopy of *T. testudinum*, and that leaf breakage increased when the *T. testudinum* canopy was removed. Based on these findings, we expect that the extent of seagrass beachings at Puerto Morelos depends on the composition and spatial distribution of species in the seagrass bed, and therefore can change with time.

Second, resuspended wrack, removed from the beach, can redeposit at the beach. This resuspended wrack has reduced buoyancy due to aging, defragmentation and decomposition on the beach and in nearshore waters, and therefore, in contrast to fresh sargassum, can drift submerged. Images show wrack moving over the lagoon bottom or settling down under mild conditions. Upon Type II and Type III removal events, governed by elevated water levels, new deposits were typically observed at the beach within several days when water levels started to decrease. These deposits did not coincide with observations of fresh sargassum arrivals, suggesting the redeposition of wrack that got resuspended during the Type II and Type III events. Earlier studies have suggested resuspension and redeposition of wrack, based on data of seagrass and macroalgae wrack at beaches in Australia, Canada and Italy (Kirkman & Kendrick, 1997; Orr et al., 2005; Simeone et al., 2013). These studies observed that wrack washed away from the beach during elevated water levels due to tides or wave action, and deposited again during decreasing water levels. Simeone et al. (2013) mentioned that only small quantities of wrack redeposited, covering a small part of the beach, whereas the other studies were inconclusive about the frequency of resuspension-redeposition cycles and the amounts of wrack involved. Long-term monitoring of wrack species could give insight in the importance of wrack resuspension and redeposition and the relative abundance of seagrass.

4.3. Flushing Potential

The Puerto Morelos reef lagoon has been considered a well-flushed system with onshore flows across the reef, alongshore flows along the beach and strong return flows through the inlets (Coronado et al., 2007). As circulation is mainly wave-driven, flushing capacity increases with wave energy. Coronado et al. (2007) showed that the entire lagoon volume could be flushed in 3 h under average wave conditions ($H_s = 0.8$ m) and in only 0.35 h under hurricane conditions ($H_s = 6$ m), based on 1.5 years of measurements at the inlets and the volume of the reef lagoon. A preliminary study at the same site using numerical modeling of conservative tracers (Berriel-Bueno, 2018) also suggested this strong flushing capability of the Puerto Morelos reef lagoon. Our observations show that the wrack at the beach is removed from the swash zone during storms and is partly redeposited at the beach after days. In contrast, only a small portion of the wrack is redeposited after the extreme events of October 2020, i.e., with maximum P of 67 kW/m (3 October), 98 kW/m (7 October), and 253 kW/m (27 October). This supports the existence of a natural removal/flushing mechanism enhanced by energetic waves.

Also, the studies of Coronado et al. (2007) and Berriel-Bueno (2018) suggest that the flushing wrack rate decreases dramatically with lower energy waves. In fact with $H_s < 0.1$ m, the time needed to renew the entire water volume in the lagoon tends to infinity (Coronado et al., 2007). Under low wave energy, the

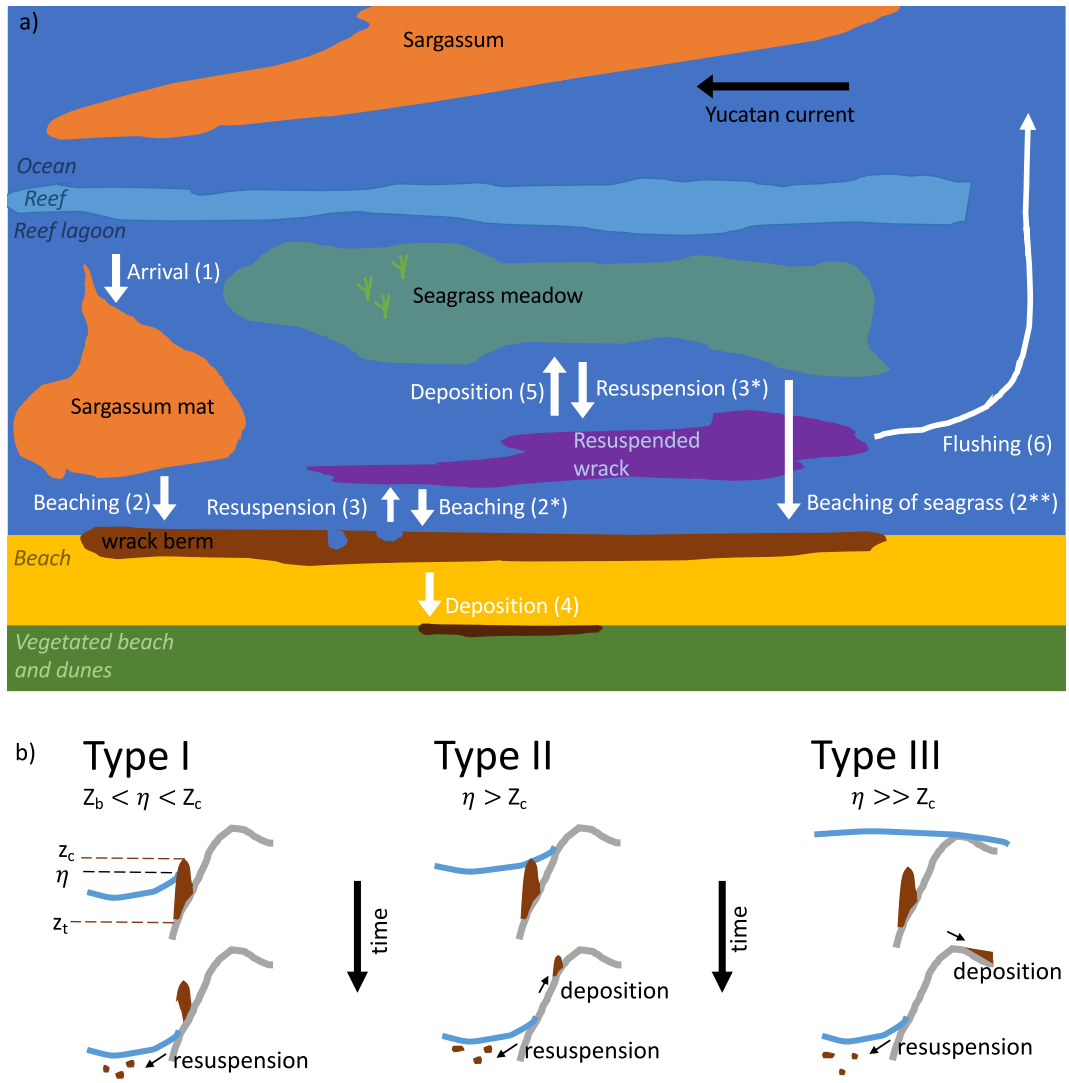

Figure 10. Conceptual model of (a) sargassum beaching and wrack dynamics and (b) wrack removal across beach profile in a reef lagoon. Numbers in panel (a) refer to the text. Only arrival (1) and beaching (2) are sequential, whereas the order of numbered processes 3–6 can differ.

sargassum wrack is expected to remain in the system and to decompose with time. Van Tussenbroek et al. (2017) observed brown-colored water when massive quantities arrived, which they explain by substantial quantities of leachates and organic particles released from sargassum wrack. This is supported by our observations. Figure 9 shows dark brown water within the arrival seasons (2018, 2019), but also in autumn (2017, 2019). The gray brown color in autumn (2017, 2019) is possibly related to the more energetic autumn waves that mix the water column, suspending organic matter and sediment. Furthermore, Van Tussenbroek et al. (2017) suggested that, based on a measured decrease in lagoon transparency and increase in seagrass leaf nutrient content, organic material was still present in the reef lagoon a year after the massive arrivals of 2014–2015. Further study is required to determine the wave climate conditions that govern the flushing rate of the wrack, as high-resolution data of the flow fields and numerical modeling are essential.

4.4. Conceptual Model

Based on the discussion above we propose a conceptual model for the nearshore sargassum dynamics in the reef lagoon of Puerto Morelos (Figure 10). Sargassum mats arrive (1) and wash ashore forming a berm (2). The wrack berm is gradually destructed during increased wave action and elevated water levels. The type

of berm destruction depends on the height of the water level η with respect to the wrack berm crest z_c and wrack berm toe z_t (Figure 10). For $z_t < \eta < z_c$ (Type I), wrack is resuspended along the seaward edge of the berm, creating small gaps in the berm that grow larger with time. For $\eta > z_c$ (Type II), the wrack berm is destructed and part of the wrack deposits on the upper beach (4) and another part is resuspended (3). For $\eta \gg z_c$ (Type III), the wrack berm is destructed and part of the wrack deposits in the dunes (4) and another part is resuspended (3). Resuspended wrack can follow three paths depending on the wave energy: beaching (again), settling on the lagoon bottom or flushing out of the lagoon. Wrack beaches again with decreasing water levels and low energy waves (2*). Advanced decomposed wrack settles on the lagoon bottom with low energy waves (5). Wrack flushes out of the lagoon with higher energy waves that enhance the reef current circulation (6). Furthermore, poststorm wrack that beaches with decreasing water levels are a combination of resuspended sargassum (2*) and storm-detached seagrass (2**), which can go again through steps (3–6).

5. Conclusions

Massive beaching of sargassum was observed at the beach of the Puerto Morelos reef lagoon (Mexico). Sargassum arrived more frequently and in larger quantities in 2018 and 2019, whereas 2017 and 2020 were moderate arrival years and 2016 a very mild year. Furthermore, the start and duration of the arrival season varied interannually. Arrivals were associated with relatively low-energetic wave and wind conditions, and onshore directed (E-SE) waves and winds. Larger sargassum mats were found to arrive with lower waves and weaker winds than smaller mats. Once sargassum beached, a berm of wrack was formed. We identified three natural removal mechanisms of the wrack berm, depending on the water level η with respect to the elevation of the berm crest z_c and berm toe z_t. For $z_t < \eta < z_c$ (Type I), the wrack berm is gradually destructed with gaps forming in the berm that grow with time, under increased wave action and a rising water level. For $\eta > z_c$ (Type II), all wrack of the berm is resuspended and part of the wrack deposits at the upper beach. Type III ($\eta \gg z_c$) is similar to Type II except that wrack deposits in the dunes instead of the upper beach, as high energy waves ($P > 39.7$ kW/m, $H_s > 2.9$ m) and extreme water levels ($\eta > 1.42$ m; 97th percentile) move the swash zone further inland. Part of the resuspended wrack is flushed out of the system when higher energy waves activate the reef circulation. Year-round wrack presence on the beach, in spite of seasonality in sargassum influx and frequent wrack removal, suggests the beaching of other plant debris (e.g., seagrass and resuspended wrack).

Acknowledgments
This project was supported by UNAM-PAPIIT TA100420 and DGAPA postdoctoral grant to J. Rutten. The Mexican National Council for Science and Technology (CONACYT) and the Universidad Nacional Autónoma de México provided financial support through projects INFR-2014-01-225,561 and Proyectos Internos Instituto de Ingeniería 5341 "Implementación de estación de video monitorización para la obtención de indicadores de vulnerabilidad a la erosión" to E. Tonatiuh Mendoza. Financial support was provided to Jaime Arriaga by the Catedras CONACYT project 1146. The authors acknowledge Servicio Académico de Monitoreo Meteorológico y Oceanográfico (SAMMO) for the collection of wind data, Miguel Ángel Gómez Reali for the collection of image data and Servicio Mareográfico for the collection of water level data. We thank Copernicus Climate Data Store for making available their model output of the ERA5 hindcast. We acknowledge Gonzalo Uriel Martín Ruiz and Juan Alberto Gómez Liera for technical support during field visits. J. Rutten acknowledges M. Tissier and A. Reniers for the financial support provided during the revision of the study. The authors thank Elizabeth Johns, Evan B. Goldstein and an anonymous reviewer for their constructive comments that led to an improved version of the manuscript.

Data Availability Statement

Hourly wave data were obtained from the Copernicus Climate Data Store (https://cds.climate.copernicus.eu/). Wind data were obtained from SAMMO (https://sammo.icmyl.unam.mx/). Water level data were obtained from Servicio Mareo-gráfico (http://www.mareografico.unam.mx/portal/). Derived image products (sargassum arrivals, wrack coverage, vegetation line, svm training pixels, and timestack) will be available from Rutten et al. (2021) after acceptance of the article.

References

Appendini, C. M., Hernández-Lasheras, J., Meza-Padilla, R., & Kurczyn, J. A. (2018). Effect of climate change on wind waves generated by anticyclonic cold front intrusions in the Gulf of Mexico. *Climate Dynamics*, *51*(9), 3747–3763. https://doi.org/10.1007/s00382-018-4108-4

Arellano-Verdejo, J., & Lazcano-Hernández, H. E. (2021). Collective view: Mapping sargassum distribution along beaches. *PeerJ Computer Science*, *7*, e528. https://doi.org/10.7717/peerj-cs.528

Arellano-Verdejo, J., Lazcano-Hernandez, H. E., & Cabanillas-Terán, N. (2019). Erisnet: Deep neural network for sargassum detection along the coastline of the Mexican Caribbean. *PeerJ*, *7*, e6842. https://doi.org/10.7717/peerj.6842

Berriel-Bueno, D. (2018). *Arribo masivo de sargazo a la laguna arrecifal de puerto morelos: Condiciones de permanencia y dispersión (Master's thesis)*. Cinvestav.

Chávez, V., Uribe-Martínez, A., Cuevas, E., Rodríguez-Martínez, R. E., van Tussenbroek, B. I., Francisco, V., et al. (2020). Massive influx of pelagic *Sargassum* spp. on the coasts of the Mexican Caribbean 2014–2020: Challenges and opportunities. *Water*, *12*(10), 2908. https://doi.org/10.3390/w12102908

Coronado, C., Candela, J., Iglesias-Prieto, R., Sheinbaum, J., López, M., & Ocampo-Torres, F. J. (2007). On the circulation in the Puerto Morelos fringing reef lagoon. *Coral Reefs*, *26*(1), 149–163. https://doi.org/10.1007/s00338-006-0175-9

Del Vecchio, S., Jucker, T., Carboni, M., & Acosta, A. T. (2017). Linking plant communities on land and at sea: The effects of *Posidonia oceanica* wrack on the structure of dune vegetation. *Estuarine, Coastal and Shelf Science*, *184*, 30–36. https://doi.org/10.1016/j.ecss.2016.10.041

Fourqurean, J. W., & Rutten, L. M. (2004). The impact of hurricane Georges on soft-bottom, back reef communities: Site-and species-specific effects in south Florida seagrass beds. *Bulletin of Marine Science*, *75*(2), 239–257.
Franks, J. S., Johnson, D. R., & Ko, D. S. (2016). Pelagic sargassum in the tropical north Atlantic. *Gulf and Caribbean Research*, *27*(1). SC6–SC11. https://doi.org/10.18785/gcr.2701.08
Franks, J. S., Johnson, D. R., Ko, D., Sanchez-Rubio, G., Hendon, J. R., & Lay, M. (2012). Unprecedented influx of pelagic sargassum along Caribbean island coastlines during summer 2011. In *Proceedings of the 64th gulf and Caribbean fisheries institute*. Puerto Morelos.
García-Sánchez, M., Graham, C., Vera, E., Escalante-Mancera, E., Álvarez-Filip, L., & Van Tussenbroek, B. I. (2020). Temporal changes in the composition and biomass of beached pelagic sargassum species in the Mexican Caribbean. *Aquatic Botany*, *167*, 103275. https://doi.org/10.1016/j.aquabot.2020.103275
Gower, J. F. R., & King, S. A. (2011). Distribution of floating sargassum in the Gulf of Mexico and the Atlantic Ocean mapped using meris. *International Journal of Remote Sensing*, *32*(7), 1917–1929. https://doi.org/10.1080/01431161003639660
Gower, J. F. R., Young, E., & King, S. (2013). Satellite images suggest a new sargassum source region in 2011. *Remote Sensing Letters*, *4*(8), 764–773. https://doi.org/10.1080/2150704X.2013.796433
Holman, R. A., & Stanley, J. (2007). The history and technical capabilities of argus. *Coastal Engineering*, *54*(6–7), 477–491. https://doi.org/10.1016/j.coastaleng.2007.01.003
Hoonhout, B. M., Radermacher, M., Baart, F., & Van der Maaten, L. J. P. (2015). An automated method for semantic classification of regions in coastal images. *Coastal Engineering*, *105*, 1–12. https://doi.org/10.1016/j.coastaleng.2015.07.010
Hu, C., Murch, B., Barnes, B. B., Wang, M., Maréchal, J.-P., Franks, J., et al. (2016). Sargassum watch warns of incoming seaweed. *Eos*, *97*, 10–15. https://doi.org/10.1029/2016eo058355
Johns, E. M., Lumpkin, R., Putman, N. F., Smith, R. H., Muller-Karger, F. E., Rueda-Roa, D. T., et al. (2020). The establishment of a pelagic sargassum population in the tropical Atlantic: Biological consequences of a basin-scale long distance dispersal event. *Progress in Oceanography*, *182*, 102269. https://doi.org/10.1016/j.pocean.2020.102269
Johnson, D. R., Ko, D. S., Franks, J. S., Moreno, P., & Sanchez-Rubio, G. (2013). The sargassum invasion of the eastern caribbean and dynamics of the equatorial north Atlantic. In *Proceedings of the 65th gulf and Caribbean fisheries institute*.
Kirkman, H., & Kendrick, G. A. (1997). Ecological significance and commercial harvesting of drifting and beach-cast macro-algae and seagrasses in Australia: A review. *Journal of Applied Phycology*, *9*(4), 311–326. https://doi.org/10.1023/A:1007965506873
Maréchal, J.-P., Hellio, C., & Hu, C. (2017). A simple, fast, and reliable method to predict sargassum washing ashore in the Lesser Antilles. *Remote Sensing Applications: Society and Environment*, *5*, 54–63. https://doi.org/10.1016/j.rsase.2017.01.001
Maurer, A. S., De Neef, E., & Stapleton, S. P. (2015). Sargassum accumulation may spell trouble for nesting sea turtles. *Frontiers in Ecology and the Environment*, *13*(7), 394–395. https://doi.org/10.1890/1540-9295-13.7.394
Maurer, A. S., Stapleton, S. P., & Layman, C. A. (2019). Impacts of the caribbean sargassum influx on sea turtle nesting ecology. In *Proceedings of the 71th Gulf and Caribbean Fisheries Institute*.
Orr, M., Zimmer, M., Jelinski, D. E., & Mews, M. (2005). Wrack deposition on different beach types: Spatial and temporal variation in the pattern of subsidy. *Ecology*, *86*(6), 1496–1507. https://doi.org/10.1890/04-1486
Putman, N. F., Goni, G. J., Gramer, L. J., Hu, C., Johns, E. M., Trinanes, J., & Wang, M. (2018). Simulating transport pathways of pelagic sargassum from the equatorial Atlantic into the Caribbean Sea. *Progress in Oceanography*, *165*, 205–214. https://doi.org/10.1016/j.pocean.2018.06.009
Putman, N. F., Lumpkin, R., Olascoaga, M. J., Trinanes, J., & Goni, G. J. (2020). Improving transport predictions of pelagic sargassum. *Journal of Experimental Marine Biology and Ecology*, *529*, 151398. https://doi.org/10.1016/j.jembe.2020.151398
Rodríguez-Martínez, R. E., Medina-Valmaseda, A. E., Blanchon, P., Monroy-Velázquez, L. V., Almazán-Becerril, A., Delgado-Pech, B., et al. (2019). Faunal mortality associated with massive beaching and decomposition of pelagic sargassum. *Marine Pollution Bulletin*, *146*, 201–205. https://doi.org/10.1016/j.marpolbul.2019.06.015
Ruiz de Alegria-Arzaburu, A., Mariño-Tapia, I., Enriquez, C., Silva, R., & González-Leija, M. (2013). The role of fringing coral reefs on beach morphodynamics. *Geomorphology*, *198*, 69–83. https://doi.org/10.1016/j.geomorph.2013.05.013
Rutten, J., Arriaga, J., Montoya, L., Mariño-Tapia, I., Van Tussenbroek, B., Escalante-Mancera, E., & Appendini, C. (2021). *Image supporting data for assessment of beaching and natural removal dynamics of sargassum in Puerto Morelos*. figshare. https://doi.org/10.6084/m9.figshare.14718654
Simarro, G., Ribas, F., Alvarez, A., Guillén, J., Chic, O., & Orfila, A. (2017). Ulises: An open source code for extrinsic calibrations and planview generations in coastal video monitoring systems. *Journal of Coastal Research*, *33*(5), 1217–1227. https://doi.org/10.2112/JCOASTRES-D-16-00022.1
Simeone, S., De Muro, S., & De Falco, G. (2013). Seagrass berm deposition on a Mediterranean embayed beach. Estuarine. *Coastal and Shelf Science*, *135*, 171–181. https://doi.org/10.1016/j.ecss.2013.10.007
Torres-Freyermuth, A., Mariño-Tapia, I., Coronado, C., Salles, P., Medellín, G., Pedrozo-Acuña, A., et al. (2012). Wave-induced extreme water levels in the Puerto Morelos fringing reef lagoon. *Natural Hazards and Earth System Sciences*, *12*(12), 3765–3773. https://doi.org/10.5194/nhess-12-3765-2012
Trinanes, J., Putman, N., Goni, G., Hu, C., & Wang, M. (2021). Monitoring pelagic sargassum inundation potential for coastal communities. *Journal of Operational Oceanography*, 1–12. https://doi.org/10.1080/1755876x.2021.1902682
Valentini, N., & Balouin, Y. (2020). Assessment of a smartphone-based camera system for coastal image segmentation and sargassum monitoring. *Journal of Marine Science and Engineering*, *8*(1), 23. https://doi.org/10.3390/jmse8010023
Van Tussenbroek, B. I. (2011). Dynamics of seagrasses and associated algae in coral reef lagoons. *Hidrobiologica*, *21*(3), 293–310.
Van Tussenbroek, B. I., Hernández Arana, H. A., Rodríguez-Martínez, R. E., Espinoza-Avalos, J., Canizales-Flores, H. M., González-Godoy, C. E., et al. (2017). Severe impacts of brown tides caused by sargassum spp. on near-shore Caribbean seagrass communities. *Marine Pollution Bulletin*, *122*(1–2), 272–281. https://doi.org/10.1016/j.marpolbul.2017.06.057
Wang, M., & Hu, C. (2016). Mapping and quantifying sargassum distribution and coverage in the central West Atlantic using MODIS observations. *Remote Sensing of Environment*, *183*, 350–367. https://doi.org/10.1016/j.rse.2016.04.019
Wang, M., Hu, C., Barnes, B. B., Mitchum, G., Lapointe, B., & Montoya, J. P. (2019). The great Atlantic sargassum belt. *Science*, *365*(6448), 83–87. https://doi.org/10.1126/science.aaw7912
Webster, R. K., & Linton, T. (2013). Development and implementation of sargassum early advisory system (seas). *Shore and Beach*, *81*(3), 1.
Williams, S. L. (1987). Competition between the seagrasses *Thalassia testudinum* and *Syringodium filiforme* in a Caribbean lagoon. *Marine Ecology Progress Series*, *35*, 91–98. https://doi.org/10.3354/meps035091